Subsurface residual stress and damaged layer in high-speed grinding considering thermo-mechanical coupling influence

Zhida Ren (13917423585@163.com)
Donghua University https://orcid.org/0000-0003-0645-2449
Beizhi Li
Qingzhi Zhou

Research Article

Keywords: high-speed grinding, residual stress, damaged layer, thermo-mechanical influence

Posted Date: February 15th, 2022

DOI: https://doi.org/10.21203/rs.3.rs-1350935/v1

Subsurface residual stress and damaged layer in high-speed grinding considering thermo-mechanical coupling influence

Zhida Ren, Beizhi Li*, Qingzhi Zhou

College of Mechanical Engineering, Donghua University, Shanghai 201620, China

*Corresponding author: Beizhi Li

E-mail address: lbzhidhu@163.com

Abstract: Subsurface residual stress and damaged layer play a vital role in determining the accuracy maintenance and fatigue performance of parts. Due to the advantages of machining quality and efficiency, high-speed grinding technology is being applied to the machining of precision parts. At present, the influence of high-speed grinding on the damaged layers generation and residual stress distribution has not been completely recognized, and there has been little quantitative research on the mechanism of thermo-mechanical coupling influence on the distribution of residual stress generated in the high-speed grinding process. In this study, a finite-element model comprehensively considering grinding force and thermal field was proposed to investigate the subsurface residual stress and heat influenced layer of AISI 52100 bearing steel. The subsurface damaged layer and residual stress fields were measured to validate the analytical results. Mathematical models were proposed to quantitatively analyze the thermo-mechanical coupling influence on the distribution characteristics of subsurface residual stress. The theoretical and experimental results demonstrate that when the grinding speed surpasses the critical value of 45 m/s, the depth of residual stress and damaged layer decrease simultaneously with the increase of grinding speed. Higher grinding speeds exceeding 60 m/s are supposed to restrain the maximum value of both the tensile and compressive residual stress, which helps to enhance the precision retention and fatigue performance of components. Base on this study, the performance of the subsurface can be controlled by selecting the proper grinding speed in the high-speed range.

Keywords: high-speed grinding, residual stress, damaged layer, thermo-mechanical influence

1. Introduction

Accelerated by the high need for dependability in high-end industries, such as aviation, high-grade machine tools, and medical equipment, high-performance bearings with high reliability and long fatigue life are being demanded. As a wildly used precision finishing method of bearings, the high-speed grinding process is in achieving desired machining quality to meet high-quality part requirements. The coupling effect of thermo-mechanical produced in the grinding process induces the residual stress and damaged layer which were proved to reduce the contact fatigue strength of bearings [1]. By adopting

proper grinding parameters, the grinding surface residual stress and damaged layer can be effectively controlled. Therefore, numerous researchers have concentrated on surface integrity under the grinding speed effect [2].

Residual stress, including its distribution, is considered to be the most significant factor influencing the component performance. The residual stress is redistributed during the machining process as a result of the combined interaction of mechanical and thermal factors, which influences the fatigue behavior of components [3]. Compressive residual stress induced by grinding was found to improve contact fatigue life [4]. Deep compressive residual stress was found to be more beneficial to bearing fatigue life than shallower stress of greater magnitude [5]. The existence of residual tensile stress can accelerate the initiation of fatigue cracks and promote the crack growth rate. In addition, the greater the depth of the residual tensile stress in the subsurface, the more significant this effect is [6]. Savaria et al. [7] proposed a fatigue model considering the effect of residual stress and surface roughness on fatigue behaviors. When the model was compared to experimental data, it was discovered that residual stress had a substantial impact on fatigue behavior. Besides affecting the fatigue strength and service life, the residual stress affects the geometric shape stability of parts. The relationship between residual stress and deformation caused by weak rigid parts, especially thin-walled parts, machining was investigated by Masoudi et al. [8]. The findings indicate that residual stress difference and imbalance can enhance workpiece deformation. Thus, the effect of residual stress depth and differential on ground parts should be investigated further in the field of high-speed grinding.

The high energy consumption in grinding may result in a high temperature, causing thermal damage to the workpiece. When the temperature rises too quickly, many types of thermal damage occur. Thermal damage and heat distortion make it harder to maintain workpiece fatigue behavior and dimensional accuracy [9]. Damaged layers produced during machining differ in hardness and surface characteristics from the bulk material [10]. Extreme plastic deformation and high temperatures damage and weaken the top layer near the surface [11]. Guo et al. [12] discovered that the damaged layer has a substantial impact on the mechanical qualities of the workpiece, such as wear resistance and fatigue behavior, and that the dark layer features determine the distribution of residual stress. As a result, investigations into the damaged layers are required to enhance the workpiece's performance. The research of Zhao et al. [13] shown that the force and temperature field of grinding can be well reproduced by introducing the measured grinding wheel topography.

Grinding speed is the most important parameter in the grinding process because it has a complicated impact on thermo-mechanical load and surface integrity. High-speed grinding is becoming more popular as an efficient way of machining bearings with thin walls and long service lives. Since Salomon (1931) proposed the well-known hypothesis on high-speed machining that the temperature in metal cutting increases up to a certain point and then decreases as the cutting speed continuously rises, the advantages

of high-speed machining in controlling deformation and improving price and quality have been continually discovered. Increasing the grinding and workpiece speed, according to Ni and Li [14], may minimize phase transition and residual tension stress on the top layer. Jerolajev et al. [15] observed that the contact time and contact zone temperature during grinding had a substantial impact on the material's modification caused by the varied mechanical stresses and retained austenite. The force and heat load also have an effect on the deformed layer and residual stress throughout the machining process. The influence of grinding settings on workpiece wear-resisting property and residual stress was studied by [16]. Naskar et al. [2] claimed in their study that high-speed grinding may minimize machining forces and heat when compared to conventional methods, and that the majority of heat created during the grinding process can be dissipated by chips, resulting in a low workpiece temperature. In summary, high-speed grinding is thought to have a smaller damage layer and a more controlled residual stress distribution when compared to other machining processes. Although it is well accepted that high-speed grinding is good for controlling residual stress distribution and reducing damaged layer thickness, the interactions between the grinding-caused thermo-mechanical coupling load and residual stress indicators are still poorly understood at present.

Although numerous simulations and experiments have been carried out to study the impact of processing parameters on grinding quality, the lack of research on the complex relationship between thermo-mechanical coupling influence and grinding limits the understanding of grinding induced damaged layer and residual stress distribution mechanism. In this work, the grinding process under thermo-mechanical circumstances was examined using simulation and experimental investigation. Rather of reducing the heat source distribution into an abstract function to obviate the need for simulation, a grinding simulation model was built by explicitly simulating the topography of abrasive grain based on measurement data to obtain a more accurate temperature field and grinding force. Grinding force and heat distribution parameters were collected, and a mathematical model was proposed between them and the major indications of subsurface residual stress. The mechanisms by which heat and force influenced residual stress during grinding were investigated in both a single and combined manner. The findings of this paper's research can be utilized to demonstrate the unique mechanism and benefits of high-speed grinding, which may differ from the phenomenon observed in grinding at general speed. Fig. 1 depicts the simulation and experimental techniques used in this research. The experimentally observed subsurface damaged layers and residual stress were compared to the modeling findings. The computation of almost limitless process parameters is avoided by concentrating on the mechanism of grinding force and heat impacts on surface integrity. The impact and benefits of high-speed grinding were investigated further, and a process optimization strategy to manage residual stress and decrease damaged layer is presented. The results in this research have been partially applied in bearing manufacturing enterprises.

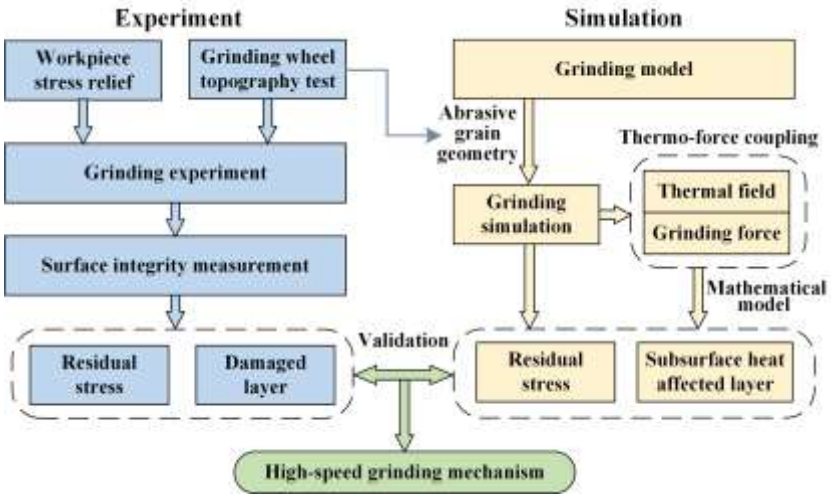

Fig. 1. Procedures for experiment and simulation

2. Experimental method

2.1 Grinding experiments

Cylindrical grinding was performed in this study. Fig. 2 depicts the experimental equipment. Grinding tests were carried out using a MQ1350B grinder. In the experiment, a 120-grit ceramic grinding wheel (120KVS) with a maximum speed of 60 m/s was employed. The topography of the grinding wheel was measured prior to the grinding tests. Each workpiece used in the experiment contains four cylindrical specimens with a diameter of Ø30 mm and a width of 15 mm so that different process parameters can be used for different specimens once the workpiece was installed.

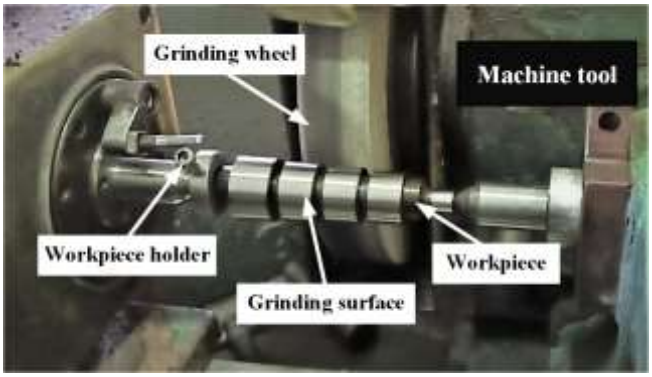

Fig. 2. Experimental equipment.

2.2 Instruments and procedures of measurement

The associated test devices and objects used in this study are shown in Fig. 3. The topography of the grinding wheel (Fig 3(a)) was measured using a KH-7700 3D Digital Microscope (Hirox Inc., USA) to reconstruct the morphology of abrasive grains.

The X-ray stress measurement system (Proton Manufacturing Ltd., USA) was used to measure the

distribution of residual stress in the subsurface using the sin2φ method (Fig 3(b)). The distribution of residual stress on the subsurface was measured by etching and polishing layer by layer and recording the thickness of the etched layer. To measure the {211} peak of the AISI52100 bearing steel, a Cr target was chosen. Five tilt angles φ of 0°, ± 7.5°and ± 15° were measured. The grinding surface was polished layer by layer (Fig 3(c)) to obtain the distribution of subsurface residual stress using a PROTO polishing device.

Microscope observations was used to determine the thickness of the subsurface damaged layers. As specimens, small pieces were cut from the machined workpieces (Fig 3(d)). With the characteristic of low hardness and poor corrosion resistance, the damaged layer will turn black after being treated by acid corrosion. The dark layer existing on the subsurface is the main damage form in the grinding process of workpieces that influence the surface integrity and weaken the contact fatigue life of parts. The specimens were coldly inlaid into samples using resin; then, to observe, cross-sections of the specimens were polished (Fig 3(e)) and etched with 7 percent Nitric acid.

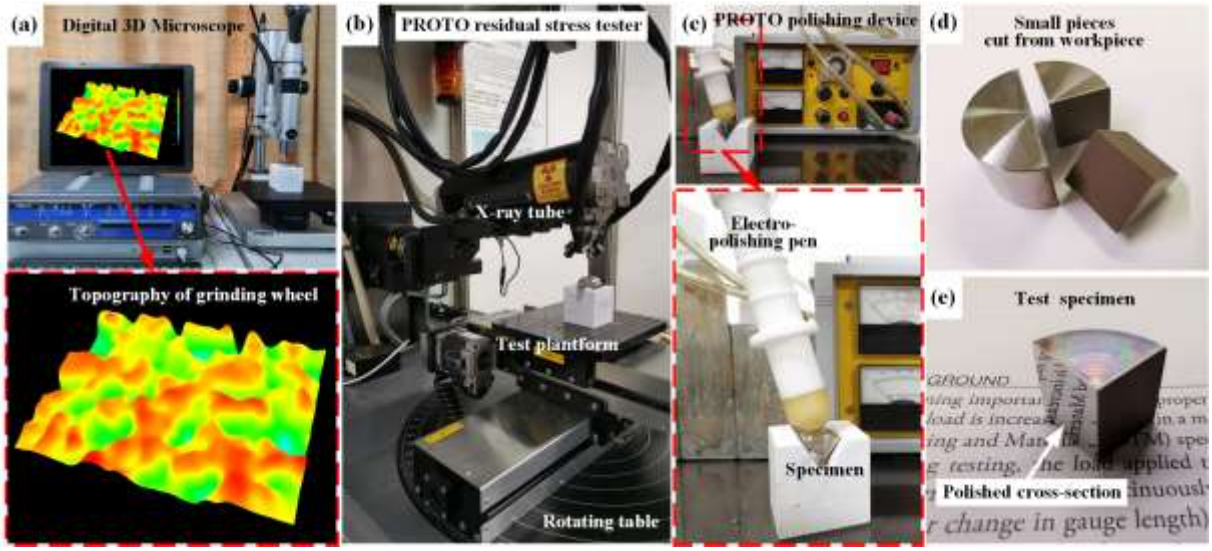

Fig. 3. Related test devices and objects. (a) grinding wheel topography detection; (b) residual stress test; (c) electro-polishing device; (d) specimens cut from workpiece; (e) test specimen.

2.3 Material and process parameters

In the grinding experiments, AISI52100 bearing steel workpieces were used, the chemical composition of which is shown in Table 1. The heat treatment procedure of workpieces is as follows: the steel is heated and quenched in oil before being tempered for 2 hours at 160 °C to reduce initial residual stress in workpieces.

The process parameters for experiments with a variable of grinding speed and constant depth of cut were established with the goal of guaranteeing machining efficiency. The maximum undeformed thickness changes as the grinding speed changes. The process parameters can be utilized to investigate

the effect of grinding speed on temperature, force, subsurface residual stress, and damaged layer in greater depth. To make the influence of grinding speed clearer and control the number of experimental group, the workpiece speed v_s was fixed at 1.57 m/s. Combinations of process parameters are obtained by selecting different parameter settings. Table 2 displays the experimental process parameter settings for grinding. Limited by the capacity of the grinding machine, grinding experiments with the wheel speed not exceeding 60 m/s were carried out (test no. 1 to 3), and all the process parameters listed were simulated in finite element software.

The damaged layer depth and residual stress are investigated at various grinding speeds and compared to the experimental findings to confirm the prediction model's correctness under the specified process parameter combination. Based on the analysis of experimental and simulation results, a further grinding speed optimization strategy can be provided.

Table 1

Chemical compositions (wt.%) of AISI 52100 steel.

Element	Cr	C	Mn	Si	Ni	P	S
Content (%)	1.4-1.6	0.98-1.10	0.25-0.35	0.2-0.3	0.08-0.12	<0.025	<0.025

Table 2

Parameters of grinding processes.

No.	Wheel speed v_s (m/s)	Depth of cut a_p (mm)	Maximum undeformed chip thickness a_{gmax} (μm)	Workpiece speed v_s (m/s)
1	30.00	0.21	6.49	1.57
2	45.00	0.14	3.60	
3	60.00	0.10	2.30	
4	75.00	0.08	1.66	
5	90.00	0.07	1.27	
6	110.00	0.06	0.93	

3. Finite element analysis

By simulating the removal of material by a single abrasive grain the machining process of high-speed grinding can be characterized, and the feasibility of this method has been fully verified by scholars[17–19]. Based on the geometric modeling of the grinding motion, the microscopic grinding parameters are determined. The formation of the residual stress field and damaged layers is significantly influenced by the thermo-mechanical coupling effect of grinding force, temperature, and their distribution field. However, it is hard to measure the grinding force, temperature, especially heat distribution field during the grinding process. Therefore, the Finite Element Method (FEM) was ultilized to simulate the grinding process so as to overcome the constraints of experimental measurement. To simulate the grinding process, the AdvantEdge™ software was used. After the grinding operation, the

thermal field in the grinding area can be analyzed, the grinding force and distribution of residual stress can be collected. Furthermore, by studying the heat impacted layer, the influence of grinding wheel speed on grinding damaged layer can be determined. Furthermore, the process of residual stress production owing to the thermo-mechanical coupling effect can be explained. The FEM was used in this work to estimate continuous residual stress distributions in a certain subsurface region. In the experiment, just a few discrete points along the depth direction were chosen for measurement. By comparing the simulation and experimental findings, the correctness of the FEM results can be confirmed.

3.1 Motion geometric model

The grinding motion geometric model was established to simulate the cylindrical grinding process shown in Fig. 4. During the grinding process, the material was separated by abrasive cutting from the workpiece. The maximum undeformed thickness $a_{g\max}$ was utilized to represent the depth of a single abrasive entering the material:

$$a_{g\max} = 2\gamma_{sl}\frac{v_w}{v_s}\sqrt{a_p\left(\frac{d_s+d_w}{d_s d_w}\right)} \tag{1}$$

where a_p is the depth of cut, d_w and d_s is the workpiece and wheel diameter, v_w and v_s is the workpiece and wheel speed and γ_{sl} is the distance of continuous cutting grit.

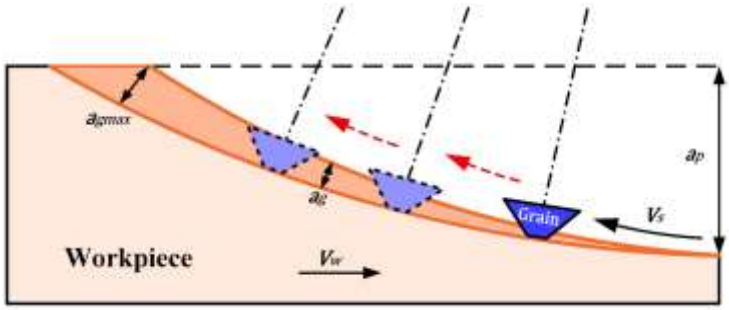

Fig. 4. Interaction mode between the abrasive grain and workpiece.

In order to make the finite element model closer to the experimental conditions and increase the reliability of the calculation results, the geometric model of abrasive grains was reconstructed based on the observation results. The dimensions of abrasive grains are obtained by measure the topography of the grinding wheel shown in Fig. 5. The detection magnification was 350 ×, and the measuring area on the wheel surface was 1.0 × 0.6 mm. The 3D topography of the abrasive grains (Fig. 5(b)) can be obtained from the selected area on the grinding wheel surface, and then cross sections of the grains (Fig. 5(c)) can be obtained by applying the cut line. According to the observation results, the cross section of abrasive grain is reconstructed into a rounded trapezoid. The continuous cutting-edge distance of abrasive grains γ_{sl}, the average radius size r, length l_g and the grain cone angle θ were obtained and calculated by using the analysis software listed in Table 3.

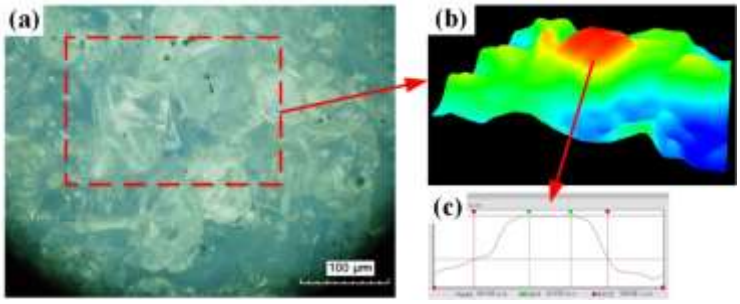

Fig. 5. Grinding wheel topography detection. (a) Distribution of abrasive grains on grinding wheel; (b) 3D topography of abrasive grain; (c) Cross section of measured abrasive grain.

Table 3

Topography parameter of the grinding wheel.

$\boldsymbol{\theta}$ (degree)	$\boldsymbol{r}$ (μm)	$\boldsymbol{l_g}$ (μm)	$\boldsymbol{\gamma_{sl}}$ (mm)
57	26	40	0.73

3.2 FE modeling

The complete process in which the workpieces contact with grains, form chips, complete grinding, and cooled to room temperature (20 ℃) spontaneously, were simulated to obtain the heat influenced layers and subsurface residual stress. A 2-D grinding FE model was created whose local enlarged image was shown in Fig. 6. The abrasive grain size and grinding settings chosen matched those performed in the experiments. The CPE4RT bilinearly displaced four-node coupled plane-strain element was used [20]. The workpiece was represented by an elastic-plastic body, whereas the tool was represented by an elastic body. The minimum mesh element sizes of workpiece and grain were 0.2 μm and 0.4 μm, respectively. The mesh on the workpiece was adaptively redivided at various stages during the simulation process. However, the refined mesh in the required depth of mesh refinement will be kept all the time instead of being coarsened to calculate the residual stress.

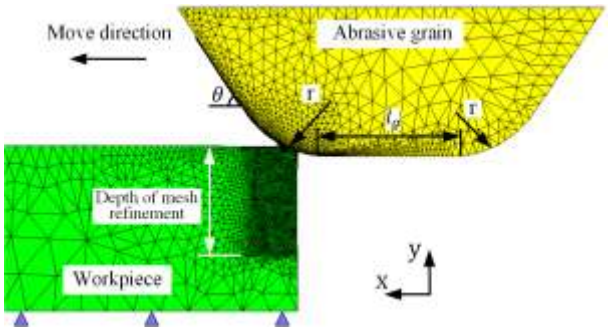

Fig. 6. FE model and boundary conditions of grinding.

As the boundary condition, the bottom of the workpiece was fixed from x and y directions. To prevent the potential of mesh distortion, the arbitrary Lagrange-Euler (ALE) method was used [21]. A fully coupled thermo-mechanical simulation was used to analyze the model. Adaptive meshing was used to model the chip generation process. The material behavior in the grinding process was described using

the Johnson-Cook (J-C) model [22]. The constitutive equation is as follows:

$$\sigma = [A + B\varepsilon^{\mathrm{n}}][1 + C\ln(\dot{\varepsilon}/\dot{\varepsilon}_0)]\{1 - [(T - T_r)/(T_m - T_r)]^m\} \quad (2)$$

where A, B, C, n, m are material constants, σ is the flow stress, $\dot{\varepsilon}/\dot{\varepsilon}_0$ is a nondimensional plastic strain rate, ε is the plastic strain, T_r is the room temperature, T_m is the material temperature. Table 4 gives the parameters of the Johnson-Cook material constitutive data.

Table 4

Parameters of Johnson-Cook material constitutive of AISI52100 [23].

$\boldsymbol{A}$ (MPa)	$\boldsymbol{B}$ (MPa)	$\boldsymbol{C}$	$\boldsymbol{m}$	$\boldsymbol{n}$
2482.4	1498.5	0.027	1.21	0.391

3.3 Simulation results

The tangential and normal grinding forces, as well as the heat distribution during grinding, were thoroughly investigated in order to determine the internal mechanism of their impacts on the formation of damaged layers and the residual stress field.

The simulation temperature fields at the wheel speed of 30, 60, and 110 m/s are selected and shown in Fig. 7. To show the heat distribution on the workpiece and abrasive grain respectively, the workpiece and abrasive are displayed separately. The common characteristics of thermal distribution show that the maximum temperature of workpiece is near the contact area with the abrasive. Some of the heat is carried away from the workpiece with chips, and most remaining heat is transferred to the inside of the material. In addition, by comparing the thermal field characteristics of workpieces under different wheel speeds, it can be found that with the increase of grinding speed the thickness of heat affected layer decreases, which leads to a smaller thickness of the damaged layer. Higher grinding speed reduces the maximum undeformed thickness of a single abrasive grain and leads to smaller plastic deformation thickness and grinding energy. Furthermore, the high-speed movement of the abrasive grain will make the heat leave the workpiece before it reaches the inside of the material. At the same time, the higher grinding wheel speed significantly reduces the influence of heat on abrasive grains, which can avoid the accumulation of heat and prolong the life of the grinding wheel.

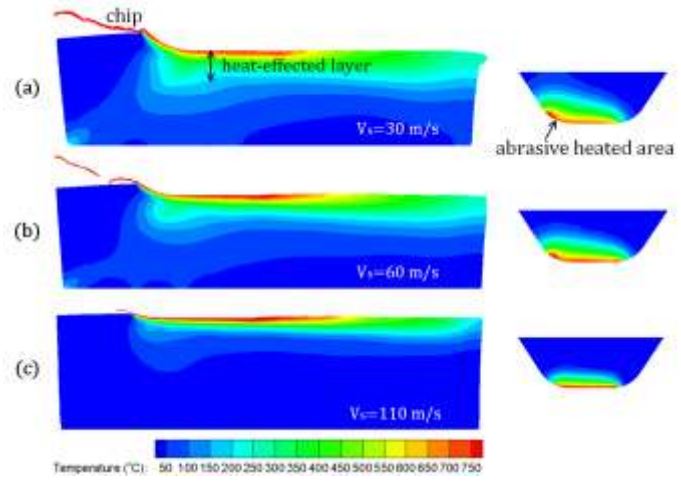

Fig. 7. The thermal fields during grinding when the grinding speeds are (a) $v_s = 30\,m/s$ (b) $v_s = 60\,m/s$ (c) $v_s = 110\,m/s$.

The tangential residual stress distribution illustrated in Fig. 8 is the result of a change in force and thermal load after grinding and cooling. The distribution of residual stress (Fig. 8(a)) shows that maximum compressive residual stress appears close to the grinding surface and below it exists tensile stress. The stress curve along the depth direction (Fig. 8(b)) extracted from FE simulation results was exemplified to illustrate the distribution of residual stress in depth. The distances from the surface to the disappearance of compressive stress d_c and tensile stress d_t are considered as the influence depth of these two kinds of residual stress. The value of d_c^* and d_t^* represents the depth of maximum compressive stress and tensile stress, respectively. Furthermore, the difference between the maximum tensile σ_t stress and maximum compressive stress σ_c is defined as the residual stress difference σ_d that can affect the deformation and accuracy retention of precision parts, especially thin-walled parts. Reducing the stress difference is conducive to control the machining deformation of thin-walled parts.

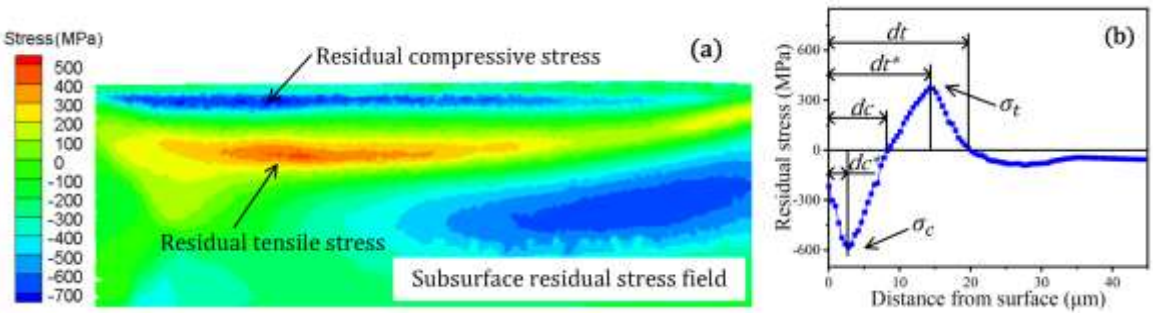

Fig. 8. Distribution of tangential subsurface residual stress. (a) residual stress field; (b) stress curve extracted from simulation results.

4. Results and discussions

4.1 Formation mechanisms of damaged layers

The simulation results of grinding force at various grinding speeds are shown in Fig. 9. The tangential force and normal force caused by abrasive grains are analyzed respectively when the grinding process is stable. Although this is generally that the grinding force decreases as the grinding speed increases, the grinding force is not completely monotonically related to the grinding speed. The normal force does not begin to decrease with the grinding speed until the grinding speed exceeds 45 m/s. A higher grinding speed can reduce the maximum micro-deformation thickness of a single abrasive particle when other process parameters remain unchanged, which plays a positive role in reducing the grinding force.

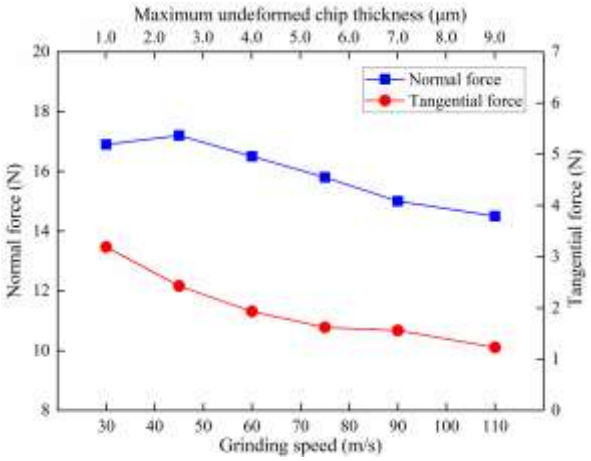

Fig. 9. Influence of grinding speed on force.

The influence of grinding speed on the thermal field is shown in Fig. 10. With the increase of grinding speed, the grinding temperature and the depth of the heat affected layer are basically decreasing. Note that the grinding temperature and thermal affected layer depth reach the maximum values when the grinding speed is 45 m/s. Since Salomon advocated a similar appearance for the first time in 1931 that the grinding heat reaches the maximum value when the grinding speed reaches a certain value and then gradually decreases, the restraining effect of high-speed machining on temperature has been continuously studied and verified [24]. For the AISI51200 bearing steel in this study, the grinding speed of 45 m/s at which the temperature will experience a turning point is determined and is verified by experiments. When the temperature exceeds the tempering temperature (150 ℃ for AISI52100 bearing steel) the material would be tempered and turn to tempered martensite, which is the cause of subsurface damage. As a consequence, the region that experienced a temperature of more than 150 °C is regarded as the damaged area. The influence of grinding speed on temperature and thermal affected layer depth is verified by measuring the thickness of damaged layer closely related with the heat change in material.

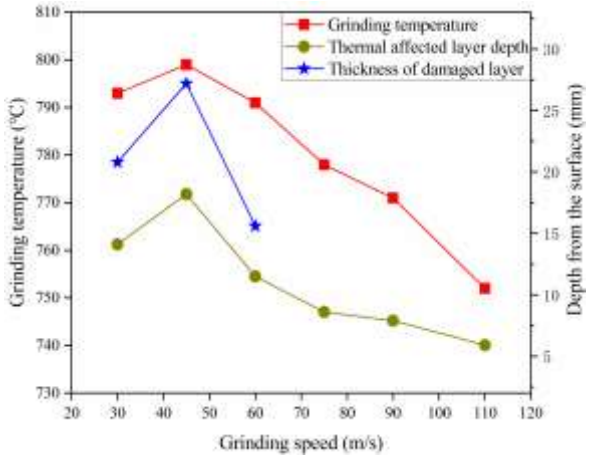

Fig. 10. Influence of grinding speed on the thermal field compared with experimental results.

Fig. 11 shows the damaged layers at different grinding speeds measured in experiments, which is used to verify the simulation results. Chou and Song [25] proved that the heat influenced depth has a significant impact on the damaged thickness in high-speed machining. The main component of the damaged layer is tempered martensite, which is caused by local grinding temperature exceeding tempering temperature. The heat in material is gradually transiting during the grinding process so the dark layer formed has a vague boundary. Although the measured damaged layers are deeper than that obtained by simulation, the consistent trend of change can be used to ensure the credibility of the simulation results. Under the condition of high-speed grinding with the grinding speed exceeding 45 m/s, the temperature and damaged layer thickness decrease with the increase of speed. The opposite situations occur when the grinding speed is less than 45 m/s. High-speed grinding leads to a phenomenon the excess heat is removed before it transfers to the inside of the material.

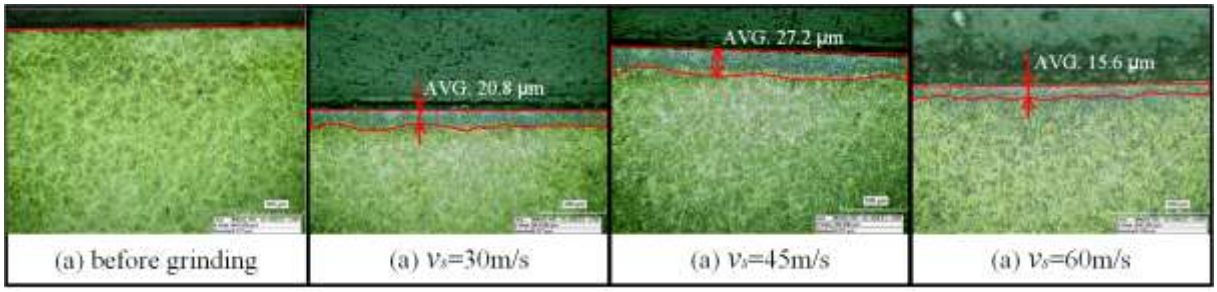

Fig. 11. Depth of damaged layers measured at different grinding speeds.

4.2 Analysis of residual stress results

The important indexes of residual stress including position, value of maximum residual stress, as well as the residual stress depth, were extracted for detailed analysis and comparison. The residual stress data were obtained from the simulation results, which were further verified by experiment results.

The comparison of residual stress depth affected by different grinding speeds was shown in Fig. 12. With the increase of wheel speed, the affected depth of residual stress and the depth of maximum

residual tend to decrease. In the above simulation findings, the fast speed of the grinding wheel results in a reduced grinding force and heat impacted depth. Compared with the low-speed grinding processes, the material experienced smaller strain and temperature rise during high-speed grinding, which lead to a shallower depth of residual stress. With the increase of grinding speed from 45 m/s to 110 m/s, the effect depth of residual tensile stress decreases by 19%. The control of residual stress distribution is beneficial to machining deformation and service life of parts. A shallow residual stress distribution depth is beneficial to control machining deformation and precision stability of parts, especially thin-walled parts. At the same time, controlling the distribution depth of residual tensile stress can reduce the propagation rate of fatigue cracks on the subsurface and prolong the fatigue life.

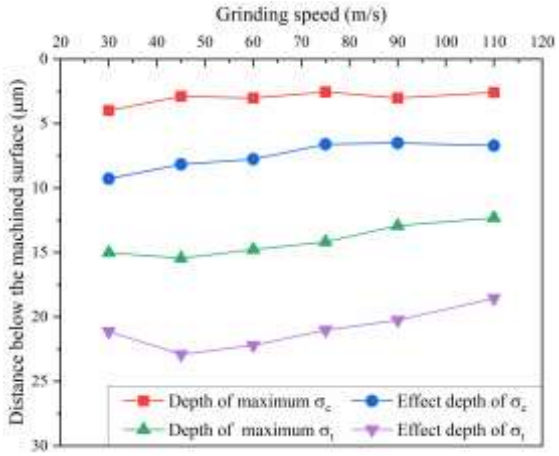

Fig. 12. Influence of grinding speed on residual stress depth.

In contrast, the influence of grinding wheel speed on the maximum residual stress is close to piecewise linearity in Fig. 13. With the increase of wheel speed, the residual compressive and tensile stress first increase, and then decrease when the grinding speed exceeds 60 m/s. In fact, the thermo-mechanical coupling effect in the grinding process controls the value of residual stress. The analysis results of grinding force and heat have a similar trend to the maximum value of residual stress, that is, the force and heat load increases first and then decreases with the increase of grinding speed.

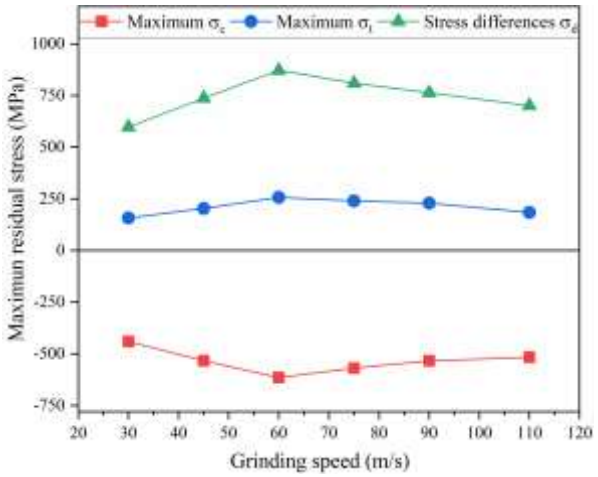

Fig. 13. Influence of wheel speed on the maximum value of residual stress.

The experimental subsurface residual stress distribution results were shown in Fig.14 whose detailed data were compared with simulation results listed in Table 5. The simulated residual stresses are greater than those of the experimental observations in absolute values. To acquire the surface residual stresses, the specimens were cut, polished, and corroded shortly after grinding, and a part of the residual stress was inevitably released during the sample preparation procedure. At the same time, the layer-by-layer polishing may make the measuring position miss the depth where the maximum stress is located. Despite this, the experimental and simulation results were generally consistent in their patterns. The average differences of the residual stress maximum value and depth between the FE results and the experiments are lower than 20%, which illustrates that the simulated residual stress pattern and magnitude agree with the test data in general.

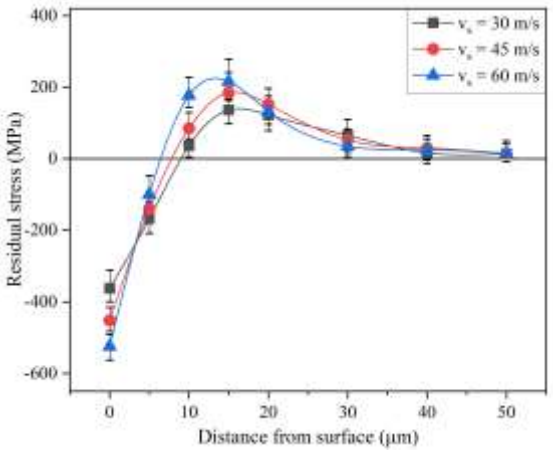

Fig. 14. Experimental subsurface residual stress.

Table 5

Difference ratio of simulated and experimental detection residual stress.

	Maximum value of residual stress (MPa)			
	Test no.	Simulation	Experiments	Difference (%)
Compressive stress	1	-440.4	-362.3	21.7
	2	-533.4	-452.4	18.0
	3	-614.7	-511.6	22.3
Tensile stress	1	157.6	136.4	15.5
	2	203.6	173.6	17.3
	3	257.1	224.8	14.3
Average difference				18.2
	Depth of residual stress (μm)			
	Test no.	Simulation	Experiments	Difference (%)
Depth of compressive stress	1	9.27	8.2	13.0
	2	8.16	7.4	10.3
	3	7.76	6.6	17.6
Depth of tensile stress	1	21.13	32.4	34.8
	2	23.12	30.1	23.3
	3	22.19	26.8	17.2
Average difference				19.3

4.3 Thermo-mechanical coupling effects on subsurface residual stress

The above analysis shows that the difference of force and heat effects during the grinding process are the direct cause of the change of surface integrity. In this section, mathematical models were formed to investigate the internal relationship between thermo-mechanical coupling effect and key indicators of residual stress, and the mechanism of high-speed grinding is further discussed.

The response surface model was defined by a polynomial function in a definite scope of independent variables. The relationships between grinding force-thermal effects and residual stress field were explored by regressively fitting the results and factors in the global scope. In this mathematical mode, grinding temperature t, thickness of heat affected layer h, normal force F_n, and tangential force F_t are selected as independent variables x. Difference of residual compressive and tensile stresses σ_d and their respective influence depth d_c and d_t are dependent variables Y.

Linear function in Eq. 3 is first tried to reflect the direct impact of each indicator on Y; if the lack of fit P-value exceeds 0.05 the second-order function in Eq. 4 will be adopted. The primary function for approximation can be formulated as the following:

$$Y = \beta_0 + \sum_{i=1}^{k} \beta_i x_i \tag{3}$$

$$Y = \beta_0 + \sum_{i=1}^{k} \beta_i x_i + \sum_{i=1}^{k} \beta_{ii} x_i^2 + \sum_{i=1}^{k} \beta_{ij} x_i x_j \tag{4}$$

In both formulae, β is the undefined coefficient, k is the quantity of designed independent variables, Y is the dependent variable, β_0 is offset items, β_i is linear offset items, β_{ii} is second-order item, β_{ij} is interaction coefficient. These coefficients are defined and estimated by the least square adjustment method, which can give a definite mathematical model when the model was proven to be effective. The following indices are used to evaluate the goodness of fit of the formula for the residual stress parameters: (1) Lack of fit P-value: the model test is significant when P<0.05. (2) Multiple-R: characterizes how well the formula fits the data which should be closed to 1.

Due to the consistent change trend, the relationship between the tangential grinding force and the depth of the residual compressive stress was expressed by a linear formula in Eq. 5. The comparison between the predicted value and the actual value was shown in Fig. 15.

$$d_c = 1.36F_t + 4.82 \tag{5}$$

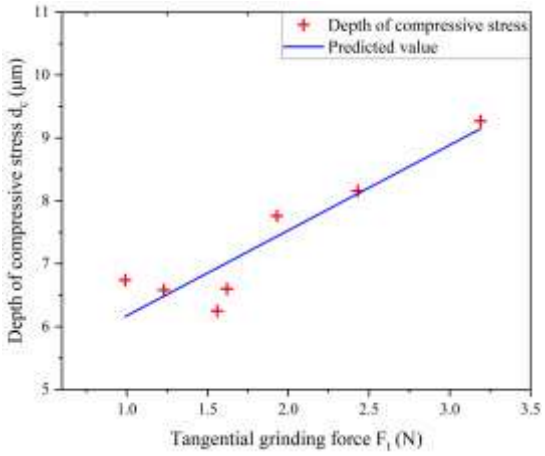

Fig. 15. Prediction model for residual stress.

The influence depth of tensile stress and stress difference are closely related to the quadratic function of force and thermal index, the second-order formulas are as follows:

$$d_t = 0.053h + 6.6 \times 10^{-5}t^2 - 0.059F_tF_n - 17.86 \quad (6)$$

$$\sigma_d = -23028F_t - 30.9F_th + 28.7F_tt + 4232.1 \quad (7)$$

Note that the P-values of coefficients of both intercept and independent in the above formulas are less than 0.05 and the Multiple-R is over 0.9.

Through the mathematical models constructed, the mechanisms of thermo-mechanical coupling effect on the distribution of subsurface residual stress can be resolved and analyzed. The depth of residual compressive stress seems to be linearly related to tangential grinding force. The tangential force causes the material to be continuously compressed during grinding and formed the plastic deformation of compression after grinding. In contrast, the thermal effect on residual compressive stress is far less than that of force. In addition, the residual tensile stress is sensitive to grinding temperature. The cooling process following grinding causes the volume of the thermally affected layer to compress, resulting in tensile stress [26]. The increase of grinding temperature or thermal influenced depth will deepen the distribution depth of residual tensile stress. Both tangential force and normal force tend to restrain the depth of residual tensile stress. In summary, the grinding mechanical loads promote the formation of residual compressive stress, and the residual tensile stress will reach the deeper area in the subsurface under the contribution of grinding heat. Furthermore, the stress difference is affected by the multiple factors of tangential grinding force, grinding temperature, and thickness of thermal influenced layer. The concentrated heat source formed by grinding can increase the stress difference. A deeper depth of thermal influence, which leads to a smaller temperature gradient, can reduce the difference between residual tensile stress and compressive stress. To minimize the residual stress difference, the heat caused by grinding can be reduced by improving cooling efficiency.

In conclusion, when the grinding speed is high enough to reach the range of high-speed grinding, the grinding force and thermal field decreases with the increase of grinding speed. Influenced by the

coupling effect of thermal and mechanical load in high-speed grinding, the reduction of residual tensile stress depth far exceeds the reduction of residual compressive stress depth. In addition, due to the reduction of temperature influence depth, smaller residual stress difference also obtained in high-speed grinding.

Furthermore, by studying the grinding essence of thermo-mechanical load, the conclusion of this study is universal and not limited by specific process parameters. Based on the simulation and experimental methods in this paper, the conclusions of this study can be extended to the grinding of other alloy carburized steels. However, the influence of grinding wheel wear on grinding quality has not been considered in this study. The research of Macerol et al. [27] shows that the wear and passivation of abrasive particles will aggravate the formation of damaged layer. The influence of phase transition can also be considered in the future to improve this study.

5. Conclusions

The influence of grinding speed on subsurface residual stress and damaged layers was evaluated using simulation and experimental research, and the particular phenomena of high-speed grinding was discussed in detail. Mathematical models were presented to characterize the process of thermo-mechanical coupling impact on subsurface residual stress, and the benefits of high-speed grinding were proven further. The following are the conclusions:

（1）When the grinding speed exceeds the critical value of 45 m/s, the grinding force and temperature decrease simultaneously with the increase of grinding speed for AISI52100 bearing steel. Furthermore, the thickness of the damaged layer generated by tempered martensite can be reduced by controlling the grinding speed in the high-speed grinding range. However, in the low-speed grinding range (v_s<45 m/s), increasing the grinding speed can aggravate the temperature and the formation of the damaged layer.

（2）The value and distribution depth of residual stress decrease can be reduced using high grinding speed (v_s>60 m/s). In this study, the depth of residual tensile stress was reduced by 19% by applying high-speed grinding. The difference between residual compressive stress and tensile stress also decreases with the increase of grinding speed, which helps to enhance the precision retention and fatigue performance of components.

（3）A mathematical model was proposed to reflect the mechanism of thermo-mechanical coupling effect on residual stress distribution. The grinding mechanical loads, tangential grinding force especially, promote the formation of residual compressive stress, and the depth of residual compressive stress is proportional to the tangential grinding force. While the residual tensile stress will reach the deeper area in the subsurface under the contribution of grinding temperature and thermal influenced depth. Therefore, to minimize the difference of residual stress, grinding parameters leading to lower

processing temperatures and good cooling conditions should be applied in the manufacture of high-performance parts.

Authors' contributions All authors participated in the work of the paper. **Zhida Ren**: methodology, data curation, investigation, software, formal analysis, visualization, writing—original draft preparation; **Beizhi Li**: validation, writing—review and editing; **Qingzhi Zhou**: supervision, resources, conceptualization. All authors have read and agreed to the published version of the manuscript.

Funding This research was financially supported by the National Key R&D Program of China (Grant No. 2018YFB1703203).

Availability of data and material The datasets used or analysed during the current study are available from the corresponding author on reasonable request.

Code availability Not applicable.

Declarations

Ethics approval Not applicable.

Consent to participate Not applicable.

Consent for publication Not applicable

Conflict of interest The authors declare no competing interests.

References

1. Moulik PN, Yang HTY, Chandrasekar S (2001) Simulation of thermal stresses due to grinding. Int J Mech Sci 43:831–851. https://doi.org/10.1016/S0020-7403(00)00027-8

2. Naskar A, Choudhary A, Paul S (2020) Wear mechanism in high-speed superabrasive grinding of titanium alloy and its effect on surface integrity. Wear 462–463:203475. https://doi.org/10.1016/j.wear.2020.203475

3. Li Y, Chen J, Wang J, et al (2020) Study on the effect of residual stresses on fatigue crack initiation in rails. Int J Fatigue 139:105750. https://doi.org/10.1016/j.ijfatigue.2020.105750

4. Zhang H, Cai Z, Chi J, et al (2021) Fatigue crack growth in residual stress fields of laser shock peened Ti6Al4V titanium alloy. J Alloys Compd 887:161427. https://doi.org/10.1016/J.JALLCOM.2021.161427

5. Matsumoto Y, Hashimoto F, Lahoti G (1999) Surface Integrity Generated by Precision Hard

Turning. CIRP Ann 48:59–62. https://doi.org/10.1016/S0007-8506(07)63131-X
6. Wang ZM, Jia YF, Zhang XC, et al (2019) Effects of Different Mechanical Surface Enhancement Techniques on Surface Integrity and Fatigue Properties of Ti-6Al-4V: A Review. Crit Rev Solid State Mater Sci 44:445–469. https://doi.org/10.1080/10408436.2018.1492368
7. Savaria V, Bridier F, Bocher P (2016) Predicting the effects of material properties gradient and residual stresses on the bending fatigue strength of induction hardened aeronautical gears. Int J Fatigue 85:70–84. https://doi.org/10.1016/J.IJFATIGUE.2015.12.004
8. Masoudi S, Amini S, Saeidi E, Eslami-Chalander H (2015) Effect of machining-induced residual stress on the distortion of thin-walled parts. Int J Adv Manuf Technol 76:597–608. https://doi.org/10.1007/s00170-014-6281-x
9. Krauss G (2017) Tempering of Lath Martensite in Low and Medium Carbon Steels: Assessment and Challenges. Steel Res Int 88:. https://doi.org/10.1002/SRIN.201700038
10. Guo YB, Sahni J (2004) A comparative study of hard turned and cylindrically ground white layers. Int J Mach Tools Manuf 44:135–145. https://doi.org/10.1016/J.IJMACHTOOLS.2003.10.009
11. Umbrello D (2012) Analysis of the white layers formed during machining of hardened AISI 52100 steel under dry and cryogenic cooling conditions. Int J Adv Manuf Technol 2012 645 64:633–642. https://doi.org/10.1007/S00170-012-4073-8
12. Guo YB, Warren AW, Hashimoto F (2010) The basic relationships between residual stress, white layer, and fatigue life of hard turned and ground surfaces in rolling contact. CIRP J Manuf Sci Technol 2:129–134. https://doi.org/10.1016/J.CIRPJ.2009.12.002
13. Zhao B, Guo X, Bie W, et al (2020) Thermo-mechanical coupling effect on surface residual stress during ultrasonic vibration-assisted forming grinding gear. 59:19–32
14. Ni J, Li B (2012) Phase transformation in high-speed cylindrical grinding of SiC and its effects on residual stresses. Mater Lett 89:150–152. https://doi.org/10.1016/J.MATLET.2012.08.119
15. Jermolajev S, Epp J, Heinzel C, Brinksmeier E (2016) Material Modifications Caused by Thermal and Mechanical Load During Grinding. Procedia CIRP 45:43–46. https://doi.org/10.1016/J.PROCIR.2016.02.159
16. Zoei MS, Sadeghi MH, Salehi M (2016) Effect of grinding parameters on the wear resistance and residual stress of HVOF-deposited WC–10Co–4Cr coating. Surf Coatings Technol 307:886–891. https://doi.org/10.1016/J.SURFCOAT.2016.09.067
17. Pang J, Wu C, Wang Q, Li B (2018) Modeling of grinding wheel topography based on a joint method of 3D microscopic observation and embedded grindable thermocouple technique. Int J Adv Manuf Technol 2018 971 97:25–37. https://doi.org/10.1007/S00170-018-1892-2
18. Ding Z, Sun J, Guo W, et al (2021) Thermal Analysis of 3J33 Grinding Under Minimum Quantity Lubrication Condition. Int J Precis Eng Manuf Technol 2021 1–19. https://doi.org/10.1007/S40684-

021-00391-Y
19. Wu C, Pang J, Li B, Liang SY (2019) High-speed grinding of HIP-SiC ceramics on transformation of microscopic features. Int J Adv Manuf Technol 2019 1025 102:1913–1921. https://doi.org/10.1007/S00170-018-03226-4
20. Ding Z, Sun G, Guo M, et al (2020) Effect of phase transition on micro-grinding-induced residual stress. J Mater Process Technol 281:116647. https://doi.org/10.1016/j.jmatprotec.2020.116647
21. Zhang F, Duan C, Sun W, Ju K (2019) Effects of cutting conditions on the microstructure and residual stress of white and dark layers in cutting hardened steel. J Mater Process Technol 266:599–611. https://doi.org/10.1016/j.jmatprotec.2018.11.038
22. Su J (2006) RESIDUAL STRESS MODELING IN MACHINING PROCESSES
23. Wang W, Salvatore F (2020) Characteristic assessment and analysis of residual stresses generated by dry belt finishing on hard turned AISI52100. 59:11–18. https://doi.org/10.1016/j.jmapro.2020.09.039
24. Su G, Xiao X, Du J, et al (2020) On cutting temperatures in high and ultrahigh-speed machining. Int. J. Adv. Manuf. Technol. 107:73–83
25. Chou YK, Song H (2005) Thermal modeling for white layer predictions in finish hard turning. 45:481–495. https://doi.org/10.1016/j.ijmachtools.2004.09.006
26. Fereiduni E, Banadkouki SSG (2014) Ferrite hardening response in a low alloy ferrite – martensite dual phase steel. J Alloys Compd 589:288–294. https://doi.org/10.1016/j.jallcom.2013.11.183
27. Macerol N, Franca LFP, Krajnik P (2020) Effect of the grit shape on the performance of vitrified-bonded CBN grinding wheel. J Mater Process Technol 277:. https://doi.org/10.1016/j.jmatprotec.2019.116453